International Journal of Bioprinting

RESEARCH ARTICLE

3D bioprinting of corneal decellularized extracellular matrix: GelMA composite hydrogel for corneal stroma engineering

Mingshan Zhang[1,2,3†], Fang Yang[4,5†], Daobo Han[1†], Shi-yao Zhang[4], Yipeng Dong[1], Xinyu Li[4], Liyun Ling[4], Zhichao Deng[1], Xuewei Cao[1], Jianguo Tian[1], Qing Ye[1,3*], Yan Wang[4,6*]

[1]Key Laboratory of Weak-Light Nonlinear Photonics, Ministry of Education, School of Physics and TEDA Applied Physics, Nankai University, Tianjin, China

[2]Institute of Modern Optics, Eye Institute, Nankai University, Tianjin, China

[3]Nankai University Eye Institute, Nankai University Afflicted Eye Hospital, Nankai University, Tianjin, China

[4]Clinical College of Ophthalmology, Tianjin Medical University, Tianjin, China

[5]Department of Ophthalmology, Renmin Hospital, Hubei University of Medicine, Shiyan, China

[6]Tianjin Eye Hospital and Nankai University Eye Institute, Tianjin Key Lab of Ophthalmology and Visual Science, Tianjin Eye Institute, Nankai University Affiliated Eye Hospital, Nankai University, Tianjin, China

[†]These authors contributed equally to this work.

***Corresponding authors:**
Qing Ye
(yeqing@nankai.edu.cn)

Yan Wang
(wangyan7143@vip.sina.com)

Citation: Zhang M, Yang F, Han D, *et al*., 2023, 3D bioprinting of corneal decellularized extracellular matrix: GelMA composite hydrogel for corneal stroma engineering. *Int J Bioprint,* 9(5): 774.
https://doi.org/10.18063/ijb.774

Received: March 3, 2023
Accepted: April 27, 2023
Published Online: June 14, 2023

Abstract

Millions of individuals across the world suffer from corneal stromal diseases that impair vision. Fortunately, three-dimensional (3D) bioprinting technology which has revolutionized the field of regenerative tissue engineering makes it feasible to create personalized corneas. In this study, an artificial cornea with a high degree of precision, smoothness, and programmable curvature was prepared by using digital light processing (DLP) 3D bioprinting in one piece with no support structure, and the construct was then confirmed by optical coherence tomography (OCT). On the basis of this approach, we developed a novel corneal decellularized extracellular matrix/gelatin methacryloyl (CECM-GelMA) bioink that can produce complex microenvironments with highly tunable mechanical properties while retaining high optical transmittance. Furthermore, the composite hydrogel was loaded with human corneal fibroblasts (hCFs), and *in vitro* experiments showed that the hydrogel maintained high cell viability and expressed core proteins. *In vivo* tests revealed that the hydrogel might promote epithelial regeneration, keep the matrix aligned, and restore clarity. This demonstrates how crucial a role CECM plays in establishing a favorable environment that encourages the transformation of cell function. Therefore, artificial corneas that can be rapidly customized have a huge potential in the development of *in vitro* corneal matrix analogs.

Keywords: Corneal decellularized extracellular matrix; Digital light processing; Gelatin methacryloyl; Double-curvature structure; Human corneal fibroblasts

1. Introduction

As the outermost protective barrier of the eye, the cornea provides important functions of the visual system, such as optical refraction, visual transparency, and biomechanical protection. Moreover, the cornea is easily damaged by corneal diseases or external trauma, which cause blindness in severe cases. Currently, the most effective treatment option is corneal transplantation. Although surgical equipment and techniques are constantly innovating, the cure rate of corneal diseases is still limited by the critical shortage of donor corneas, receptor rejection, and complications[1,2]. To address the challenge of severe shortages, the study of corneal substitutes has become a popular topic of research concerning ocular tissue engineering.

With the rapid development of tissue scaffold fabrication techniques, three-dimensional (3D) printing technology has gradually turned into a powerful tool for tissue engineering[3] and is widely used for the fabrication of artificial skin[4], cartilage[5], blood vessels[6], liver[7], and other organs and tissue. Due to the availability of various material options, inkjet and extrusion bioprinting technologies are widely used in corneal tissue engineering[8,9]. Yet adopting such techniques still results in low resolution (hundreds of μm scale) in artificial corneal printing. The use of small nozzles to improve resolution inevitably compromises cell viability[10]. The point-to-point curing method also reduces printing speed and necessitates intricate post-processing, which restricts their scalability[11], ultimately affecting the structure and function of the artificial cornea. The digital light processing (DLP) bioprinting platform is based on digital micromirror devices (DMDs) for two-dimensional (2D) projection to achieve precise control of photopolymerization of biological materials at predetermined locations. This significantly increases printing speed and indicates that system resolution is no longer limited by nozzle size, deposition time, and additional external consumables[12-14]. At the same time, DLP bioprinting technology uses a low-energy ultraviolet light source (<20 mw/cm^2), which can reduce cell damage and achieve the need for high cell survival rate and high cell density. As a result, DLP bioprinting technology allows for precise control of cells and biomaterials to produce a functional structure similar to the natural corneal multilayer hyperbolic structure.

In combination with being architecturally biomimetic, it is essential to develop biomaterials that mimic the biochemical microenvironment of the natural cornea. Therefore, creating biomaterials that can mimic the biochemical microenvironment is crucial. Many attempts have been made, and a variety of biomaterials have been developed for corneal engineering, including collagen (type I, type III)[15-17], silk fibroin[18], hydroxy apatite (HA), and poly(2-hydroxyethyl accelerated acrylate) (pHEMA)[19]. He *et al.* developed polyethylene glycol diacrylate/gelatin methacryloyl (PEGDA/GelMA) two-component bioink to repair corneal defects in rabbit eyes using printed multilayer structures[20]. Although these studies have their unique advantages, there are several challenges that need to be solved, such as the lack of clarity, the challenge of balancing mechanical and biocompatible properties, or the absence of extracellular matrix (ECM) components. Decellularized extracellular matrix (dECM) is an emerging biomaterial with great potential in preserving the inherent biochemical components and ultrastructure of the original ECM[15,21]. Previous studies have shown that dECM hydrogels contain a better natural tissue microenvironment than ECM-free hydrogels, inhibit inflammation, provide more sites for cell attachment, and promote tissue regeneration. Thus, dECM can serve as a bioinstructive scaffold to promote *in vivo* tissue repair and regeneration as well as to drive and regulate cellular responses such as proliferation and differentiation[17,21].

Even though dECM has a high level of biological efficacy and contains plenty of ecological sites needed by the microenvironment, single-dECM bioink cannot yet be used in the production of engineered corneal scaffolds due to low transparency[22,23], non-printability that needs to be further modified[24], and poor mechanical stability. To keep the 3D structure of the dECM in this instance, researchers have utilized a variety of strategies. For instance, a recent study has demonstrated the development of a viscous sealant for visible light activation systems based on gelatinized extracellular matrix (GelCodE)[25]. Shen *et al.* utilized hyaluronic acid methacrylate (HAMA) to bind to porcine corneal decellularization matrix (pDCSM-G) to obtain a mechanically enhanced and biologically stable bi-network hydrogel for the treatment of corneal defects[26]. Furthermore, prior studies have indicated that, despite the ability in enhancing printability, HAMA as well as other modified derivatives were not conductive to cell adhesion[27]. Meanwhile, compared to biologically inert synthetic materials, natural materials have good biocompatibility. Recently, a clinical study revealed that purified medical-grade type I porcine collagen stromal tissue had a positive effect on advanced keratoconus vision restoration with minimally invasive surgery, as demonstrated in two clinical cohorts[28]. However, this condition does not allow for personalization or requires resource- and time-consuming mold creation based on different geometric traits of the patients. GelMA is an excellent option for ensuring biocompatibility and enhancing the material's crosslinkability, while having highly adjustable mechanical

properties. Moreover, it shows high abilities to generate tissue substitutes and *in vitro* experimental models. Since printability and biocompatibility are necessary for bioink design, the combination of tissue-matched dECM and GelMA hydrogels will offer a favorable microenvironment for cell maturation and performing critical functions[11,29,30].

In this work, we created a freeform methodology to produce a double-curvature corneal structure by using a high-precision, fast-manufactured, homemade DLP 3D bioprinting system (Figure 1). The shape or dioptric capability of the cornea can be customized in the absence of external consumables. For corneal tissue engineering, we created a practical bioink based on GelMA and fused corneal decellularized extracellular matrix (CECM). Then, we confirmed its printing and physicochemical capabilities. Based on the results of various aspects, the composite hydrogels clearly have better key qualities. The addition of CECM optimized the mechanical properties and caused the physical characterizations of the substitutes to be closer to those of their natural counterparts. Furthermore, we used this method to develop biomimetic CECM-GelMA corneal stroma constructs loaded with human corneal fibroblasts (hCFs) to guide cellular organization while simulating the biochemical microenvironment necessary to encourage the secretion of crucial proteins unique to corneal keratocytes and the induction of physiological morphology[31,32]. Hence, the method we proposed eases the customization of artificial corneas and increases the collection of cornea-specific bioinks for DLP 3D printing, offering a promising strategy for corneal substitute research in the future that can be a foundation in simulating natural ECM and regenerative medicine.

2. Materials and methods

2.1. Preparation of CECM-GelMA bioink

Fresh porcine corneas were removed from the porcine eyeball, which was taken from the local slaughterhouse. The surface of the porcine cornea with foreign bodies was cleaned using phosphate-buffered saline (PBS). The epithelial and endothelial layers were dissected to obtain a complete corneal stroma layer. The stroma layer was sliced into several pieces, stirred in 0.5% (w/v) Triton X-100 (Sigma, USA) solution at 37°C for 6 h, and rinsed 3 times with PBS. After soaking in 1% (w/v) sodium dodecyl sulfate (SDS) for 12 h, the tissue was washed with 1× PBS and 75% ethanol for 2 h and 12 h, respectively. Then, the tissue was soaked in 1× PBS containing 1% (v/v) penicillin–streptomycin for 2 h. All the above solutions were filtered through a 0.22-μm filter to achieve sterilization. Hematoxylin–eosin (HE) staining and deoxyribonucleic acid (DNA) content tests were performed to confirm that the corneas were actually decellularized. The results are shown in **Figure S1** (Supplementary File). After that, the tissue was lyophilized overnight in a vacuum freeze-drying system (CoolSafe 55-4, Scanlaf, Denmark) sterilized by ultraviolet (UV) light. After using a bioclean 3D frozen grinding machine (KZ-5F-3D, Servicebio, China) to grind the tissue in a 3D low-temperature environment, CECM powder was formed. Then, the powder was dissolved in 0.5 M acetic acid with 2 mg/mL pepsin solution over 3 days. Completing the above steps, we prepared a 2% (w/v) CECM solution and stored it at 4°C for further use. In this study, photoinitiator (Irgacure 2959 used in bioink without cells; lithium phenyl (2,4,6-trimethylbenzoyl) phosphinate (LAP) used in cell-loaded bioink) was first dissolved in PBS and shaken at 50°C for 30 min. Tartrazine (MCE, USA) was added to the prepolymer as a light absorber to adjust the printing accuracy of the z-axis. GelMA (M299513, Aladdin, China) was weighed and dissolved in the solution containing the photoinitiator and light absorber, and rocked at 50°C. A 50-μm nylon filter membrane was used to filter the CECM solution. The pure CECM solution was obtained by centrifuging at 2500 rpm for 15 min to remove impurities and particles. Then, 10 M NaOH solution was added dropwise to the CECM solution until the pH stabilized at approximately 7.4. The pH-adjusted CECM solution was mixed with GelMA solution to form CECM-GelMA composite bioinks. The final concentration of the bioink was 10% (w/v) GelMA, 0.5% (w/v) photoinitiator, 0.02% (w/v) tartrazine, and 0.5%–1% (w/v) CECM.

2.2. DLP 3D printing system configuration

According to Figure 1A, a pull-up DLP 3D printing system was developed, which had been mainly divided into three parts: optical homogenization system, digital dynamic mask projection system, and photopolymerizable printing platform system. In the homogenization section, an LED light source with adjustable light power was employed and collimated by a UV-grade fused silica lens to uniformly illuminate DMD (1024 × 768; Texas Instrument, USA). In the state of DMD, different transmission patterns were reflected into the projection part. Light from the illumination optics was converged to the projection optics through a biconvex lens. The 2× infinite objective lens was used to ensure clear imaging and uniform brightness. The photopolymerizable printing platform consists of a bottom transparent liquid tank, a build plate, and a mechanical part, which includes a motorized translation stage, a temperature controller, and a pressure sensor. In this part, considering the patterns projected by DMD onto the prepolymer plane from the bottom, a UV-nonabsorbent and release film was stretched at the bottom of the liquid tank. To ensure the position of the initial plane at the beginning of printing, the film was attached to a UV-grade fused silica flake as a rigid window under which the pressure sensor was placed. The

build plate was fixed on the motorized linear translation stage above the liquid tank so that it could move freely in the z direction. The 3D-printed structure could be cured layer by layer and lifted by the movable build plate. Since most of the current bioinks are thermosensitive materials, the heating device must be equipped with a 3D printer that can keep the prepolymer in a solution state and maintain fluidity at all times. All the 3D printer components are located on the optical breadboards. To prevent dust and biological pollution, the entire system is placed in a biosafety cabinet (BSC-1100IIA2-X; Biobase, China) to ensure that the biological manufacturing process of the environment is clean.

2.3. Optical coherence tomography test

The target 3D model was designed and cut into a series of evenly spaced 2D images using software. The engineered image produced by DMD was used to generate a dynamic mask. Depending on the modulation of the DMD, the illuminating beam forms an image on the surface of the prepolymer through the projection lens assembly. The illuminated areas solidify, while the dark areas remain in the liquid phase. The power of the LED with a 365 nm wavelength was set to 18 mW/cm^2 so that the UV crosslinking energy was directly controlled by adjusting the exposure time. Through layer-by-layer polymerization, microstructures with intricate geometric shapes were formed. Then, the curvature of the sample was measured by optical coherence tomography (OCT; Telesto® SD-OCT; Thorlabs, USA).

2.4. Characterization of the composite hydrogels

2.4.1. Rheological examination

An modular intelligent rheometer (MCR302; Anton Paar, Austria) was used to investigate the rheological behavior of each gel. The storage modulus (G′) and loss modulus (G″) were measured in oscillation mode. For kinetic investigations, the cylindrical hydrogel samples (d = 30 mm, h = 3 mm) were set between parallel plates (d = 3 mm) starting the measurement with a fixed strain (0.3 N) and a shear rate ranging from 0.1 rad/s to 100 rad/s at room temperature (RT). The viscosities of both CECM-GelMA and pure GelMA hydrogels were calculated.

2.4.2. Compression examination

The mechanical properties of hydrogels were measured using an FGP-5 dynamometer (SHIMPO, Japan) equipped with a displacement measuring stand (mm level). The cylindrical hydrogel (r = 5 mm, h = 3 mm, n = 3) samples were fabricated using a DLP 3D printing system and tested for uniaxial loading with a maximum compressive strain of 90%. A force–displacement curve of the stress recorded with a compression step size of 0.1 mm was acquired. In the process of stress–strain measurements, a charge-coupled device (CCD) placed under the samples was used to monitor the area in real time. The elastic modulus in the linear region and ultimate compressive strength of the samples were calculated according to the method reported previously[33] as Equation I:

$$Compressive\ modulus = \frac{\sigma}{\varepsilon} \quad (I)$$

where σ is the stress (the applied force divided by the cross-sectional area) and ε is the strain (the moving distance divided by the initial thickness of the sample).

2.4.3. Light transmission examination

A high-resolution spectrometer (HR4000, Ocean Optics, USA) was used to test the transmittance of the manufactured hydrogels (r = 3 mm, h = 1 mm) and human corneal stroma (r = 3 mm, h = 150 μm). Human corneal stromal tissue was obtained from small incision lenticule extraction (SMILE) surgery at Tianjin Eye Hospital, Tianjin Medical University. Patients (age: 20–40 years) donated lenticules after SMILE surgery (stromal lenticule diameter of 6.0 mm, thickness of 80–150 μm) after informed consent was obtained from the patients. The samples were placed in a glass-bottomed dish with a coverslip placed on the surface to ensure flatness. The light emitted from the xenon lamp was collimated and passed through the sample, which was finally collected by the spectrometer. Transmission spectra in the visible band were obtained. By using a blank set as a reference, the transmittance values were corrected and subsequently normalized for thickness. The transmittance was determined using Equation II:

$$T = \frac{I}{I_0} \quad (II)$$

where T is the transmittance, I is the transmitted light intensity, and I_0 is the initial light intensity.

2.4.4. Swelling characteristics and equilibrium water content testing

The swelling degree of GelMA hydrogels with and without CECM was measured by weighing the lyophilized and swelled masses using an electronic balance. The dry weight of the hydrogel samples produced by 3D printing (r = 5 mm, h = 3 mm) was calculated (W_d). The lyophilized samples were immersed in PBS and incubated for 24 h at 37°C. The samples were removed from PBS, and their surface was gently blotted dry with filter paper. Then, the wet weight (W_w) at 1, 2, 3, 6, and 24 h was recorded. The swelling rate was calculated as Equation III:

$$Swelling\ rate = \frac{(W_w - W_d)}{W_d} \quad (III)$$

The equilibrium water content of the gel samples was calculated according to Equation IV:

$$EWC = \frac{(W_w - W_d)}{W_w} \quad \text{(IV)}$$

2.4.5. In situ and enzymatic degradation

The 3D-bioprinted samples (n = 3) were lyophilized overnight at -50°C under 200 mbar pressure in a freeze dryer (Scanlaf, Denmark). The hydrogels were soaked with distilled water at RT to constant weight, and then the initial mass of the samples (W_0) was recorded. The samples were then reincubated in PBS for 1, 2, 3, and 4 h to determine the residual mass (W_r). The *in situ* deterioration was computed as Equation V:

$$R_s = \frac{W_r}{W_0} \quad \text{(V)}$$

The enzymatic degradation of different samples was evaluated using collagenase type I (BS163; Biosharp, China). The incubated hydrogel samples were weighed to obtain W_0 and then soaked in type I collagenase solution (10 U/mL, in PBS). At various intervals, the residual mass (W_w) was measured (1, 2, 3, and 4 h). The degree of collagenase degradation was determined using Equation VI:

$$R_e = \frac{W_w}{W_0} \quad \text{(VI)}$$

2.5. *In vitro* study

2.5.1. Cultivation of human corneal fibroblasts

In accordance with ethics approval from Tianjin Eye Hospital, human corneal stromal tissue was obtained from lenticule leftovers from SMILE surgery. The donated lenticules were immediately immersed in PBS and then cut into pieces. DMEM/F12 medium with 2 mg/mL collagenase I was used to digest the tissue and single cells. The isolated cells were cultured in DMEM/F12 medium containing 10% fetal bovine serum, 1% penicillin–streptomycin, and 1% amphotericin B in a 5% CO_2 incubator at 37°C. Cell passage was carried out when 80% of the cells in the petri dish were conjoined. Cells in passages 3–5 were used for the following experiments. All experiments were approved by the Ethics Committee of Tianjin Eye Hospital, China (No. 2021-024).

2.5.2. Cell loading in GelMA and CECM-GelMA hydrogels

For the 3D cell printing of cell-laden constructs, GelMA was dissolved in PBS or neutralized CECM solution to form pure GelMA bioink and CECM-GelMA bioink with concentrations of 10% (w/v) GelMA, 1% (w/v) CECM, and 0.5% (w/v) LAP. hCFs were digested with 0.05% trypsin-EDTA (Sigma–Aldrich, USA) and centrifuged. Then, the cells were resuspended in each type of bioink with a prepolymer cell density of 1.0×10^5 cells/mL. hCF-containing bioinks were used for DLP 3D printing to manufacture cell-loaded hydrogels. The hydrogels were transferred to petri dishes with growth medium (1 mL of media per dish) and incubated in a CO_2 incubator at 37°C.

2.5.3. Evaluation of cell viability

The viability of hCFs in hydrogel constructs was assessed by live/dead assay after culturing for 1, 7, and 14 days. The concentrations of the final working solution were calcein acetoxymethyl ester (Calcein-AM, 4 μM) and propidium iodide (PI, 4.5 μM) according to the Live/Dead Viability Assay Kit (CA1630-500T, Solarbio) instructions. The working solution (1 mL) was incubated with the hCF-laden hydrogel samples (r = 3 mm, h = 1 mm, n = 3) at 37°C for 25 min. A confocal microscope (TCS SP8, Leica, Germany) was then used to collect the pictures. Cell viability was calculated using the following Equation VII:

$$Cell\ viability(\%) = \frac{n_l}{n_l + n_d} \times 100 \quad \text{(VII)}$$

where n_l is the number of viable cells and n_d is the number of dead cells.

2.5.4. Immunofluorescence staining test

The printed samples containing hCFs cultured for 1, 7, and 14 days were fixed in 4% paraformaldehyde for 30 min at RT before rinsing in PBS. The samples were soaked in 0.5% Triton X-100 for 15 min to permeabilize the cells and allow the antibodies to smoothly penetrate the cells. To block the nonspecific binding sites, the samples were washed and soaked in 4% bovine serum albumin (BSA) for 1 h at RT. Fixed cells were then immunostained with lumican, α-SMA, ALDH3A1, collagen I, and vimentin antibodies. Samples were incubated in anti-lumican (1:500, Rabbit-ab168348, Abcam, UK), anti-alpha smooth muscle actin (1:500, Mouse-ab7817, Abcam, UK), ALDH3A1 polyclonal antibody (1:500, Rabbit-15578-1-AP, Proteintech, USA), anti-collagen I (1:500, Rabbit-ab260043, Abcam, UK), and anti-vimentin (1:500, Mouse-SAB4200716, Sigma, USA) antibodies overnight at 4°C. After washing three times in 4% BSA and 0.5% Triton X-100, the samples were then incubated in diluted secondary antibodies (1:500 Alexa Flour 488-conjugated AffiniPure goat anti-rabbit lgG(H+L) and Alexa Flour 647-conjugated AffiniPure goat anti-mouse lgG(H+L)) for 1 h in the dark. For nuclear staining, the hCFs were incubated with 0.1 μg/mL 4',6-diamidino-2-phenylindole (DAPI). Whole mounts were imaged using a confocal fluorescence microscope.

2.6. *In vivo* study in rabbits

2.6.1. Animal experiments

Twenty male New Zealand white rabbits weighing 2.0–2.5 kg were used as animal recipients (SCXK-2021-0020).

All animal studies were performed in accordance with the Association for Research in Vision and Ophthalmology (ARVO) Statement for the Use of Animals in Ophthalmic and Vision Research. All animal experiments were approved by the Ethical Review Committee on the Welfare of Laboratory Animals of Hubei University of Medicine, China (No. 2021-084).

The rabbits were anesthetized intravenously with 20% ethyl carbamate (1 g/kg) and topically with proparacaine hydrochloride eye drops (Alcaine, Alcon, BE). Subsequently, a partial lamellar keratectomy was created in the central cornea of the right eye of each rabbit with a 5-mm corneal trephine to approximately 1/3 the depth of the cornea, followed by blunt dissection with a mini-crescent knife (Sharpoint, UK) to create wound beds. The rabbit eyes were then evaluated using slit-lamp microscopy and anterior segment optical coherence tomography (AS-OCT, Heidelberg Engineering GmbH 69121, Inc. Heidelberg, GER) immediately after surgery. Then, the hydrogel was printed according to the OCT result of defected cornea. After that, the 3D-printed hydrogel was transplanted onto the corneal stromal bed in five rabbits (CECM-GelMA group), while the other five rabbits only received focal corneal defects without hydrogel transplant (control group). Meanwhile, nothing was done to all the left eyes (normal group). During the 2 weeks after surgery, 0.5% levofloxacin eye drops (Santen, Osaka, JPN) were applied four times per day in the operated eyes.

Each rabbit was observed daily using hand-held slit-lamp microscopy (66 visual technology, Suzhou, CHN) after surgery to assess abnormalities in the anterior segment of the eye including corneal transparency and inflammatory reactions. Pictures of rabbit eyes were taken at 1, 2, 4, and 8 weeks after surgery. In the meantime, fluorescence staining was performed, and images were taken to evaluate the defect area of the corneal epithelium. The epithelial defect (fluorescein staining area) in slit-lamp images was measured by ImageJ (n = 5), and the healing rate was calculated according to Equation VII.

$$Healing\ rate = \frac{A_0 - A_d}{A_0} \quad \text{(VII)}$$

where A_0 is the initial defect area, and A_d is the real-time defect area at different times.

2.6.2. AS-OCT test

AS-OCT was conducted and corneal thickness was immediately measured 2, 4, and 8 weeks after surgery to obtain detailed information of the corneal transverse section tissue. Two months after surgery, rabbits were euthanized, and their corneas were prepared for histological examination.

2.6.3. Histological analysis

The harvested corneas were fixed in 4% paraformaldehyde, embedded in paraffin, and sectioned before being subjected to HE and immunohis to chemical (IHC) staining. Mouse monoclonal anti-α-SMA IgG (1:300, ab7817, Abcam, UK) was used as primary antibody for IHC staining. Images were captured by Digital Slide Scanner Systems (3DHISTECH P250 FLASH, HU).

2.7. Statistical analysis

Statistical analysis was performed with GraphPad Prism 8.0. Data (average ± S.D.). Data were obtained from three independent experiments (n = 3; ns denotes $p > 0.05$, * $p < 0.05$, ** $p < 0.01$, **** $p < 0.0001$), and a t test was used depending on the number of comparisons. Statistical analysis was performed using one-way analysis of variance (ANOVA) of t test to evaluate the maximum compressive strength and failure strain. The Mann–Whitney U test was used to evaluate the Cell Counting Kit-8 (CCK-8) assay, swelling ratio, and water content. Two-way ANOVA used to evaluate other properties.

3. Results

3.1. 3D bioprinting of corneal stroma substitutes

The DLP 3D bioprinting platform based on DMD was built independently, and the system printing principle is shown in Figure 1A. To measure the lateral resolution of the 3D-printed hydrogel, a model was manufactured, as shown in Figure 1B. Therefore, the system resolution is defined as Equation VIII.

$$\bar{r} = d \cdot \sin\left(\frac{\bar{\vartheta}}{2}\right) \quad \text{(VIII)}$$

where r is the system resolution, d is the diameter of the printed center circle, and ϑ is the angle of the uncured shape.

As shown in Figure 1B captured by the optical microscope, the lateral accuracy is improved to 54.39 ± 2.6 μm. Hence, GelMA could be utilized to prepare high-precision two-dimensional structures under this 3D printing system.

The double-curvature shape of the cornea is the key to achieving the refractive function of the corneal scaffold. Subsequently, a model was built (**Figure S6** in Supplementary File) based on the average adult corneal data (R_a = 7.80 mm, R_b = 6.80 mm), and DLP 3D printing was performed on a mold-free basis to fabricate an artificial cornea with double curvature. The printed sample structure is shown in Figure 1D, which has good formability and a smooth surface. Then, the curvature of the sample was measured by OCT, and the result is displayed in Figure 1C. The center thickness of the

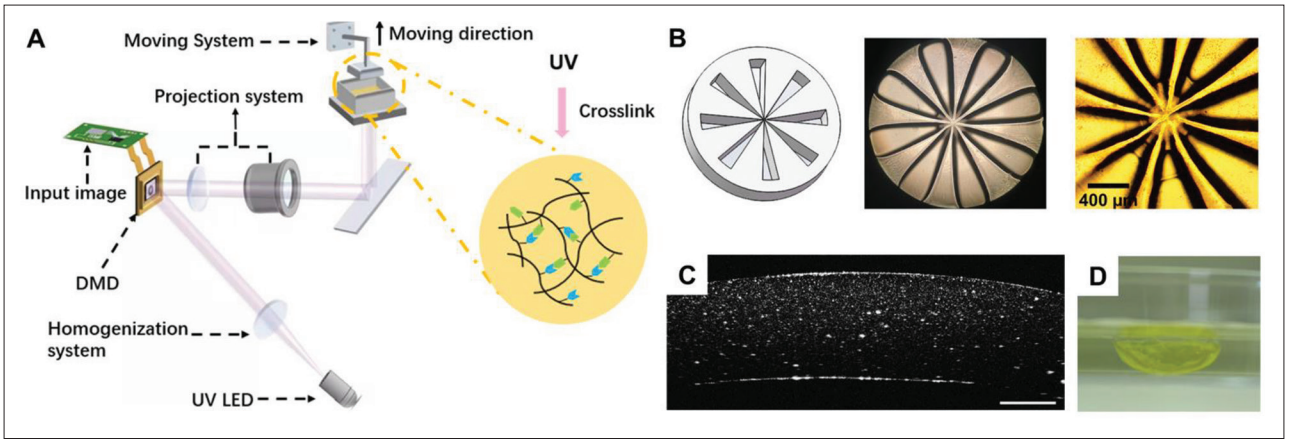

Figure 1. Shape construction of corneal stromal substitutes. (A) Schematic diagram of the DLP 3D biological printer. (B) Accuracy evaluation model of the DLP 3D printing system; overall photo and local photo of the model printed using the 3D printer under an optical microscope. (C) Optical coherence tomography image of artificial cornea with curvature formed by 0.02% tartrazine, 0.5% I2959, and 10% GelMA 3D printing. The scale bar is 500 μm. (D) Transparent bioprinted crescent-shaped artificial corneas.

structure is approximately 900 μm, and it has different internal and external curvatures. Therefore, through 3D design, individual customization can be realized, and corneal substitutes that conform to the different geometric characteristics can be prepared. Due to the addition of light absorbers, the construction structure was yellow, and the transparent hydrogel material could be seen more clearly. However, after a short period of immersion, the color was faded to obtain a hyperbolic artificial corneal structure with good transparency.

3.2. Characterization of CECM

The dECM is composed of natural substances such as collagen, glycosaminoglycan, and fibrin, which can provide physical support and a suitable microenvironment for seed cells and can induce cell adhesion and survival and realize the morphological and functional properties of the construct. Before preparing the composite hydrogels, the decellularization effect of porcine corneal stroma was evaluated. According to our HE staining results (**Figure S1A** in Supplementary File), almost all of the keratocytes were removed from the corneal tissue in the treated samples after decellularization. The tissue lacked visible cells, and extracellular matrix components were retained. Then, the decellularized tissue was tested by DNA assay (TIANcombi DNA Lyse&Det PCR Kit). The results in **Figure S1B** (Supplementary File) show that the DNA content in the decellularized tissue was 13 ng/mg, which was lower than 50 ng/mg, and was completely decellularized, avoiding adverse reactions between the cells and host and achieving good cell removal. Furthermore, the presence of CECM after hydrogel fabrication was confirmed using the Alcian blue (AB) staining (**Figure S9** in Supplementary File).

3.3. Physical and mechanical characterization of hydrogels

3.3.1. Rheological test

The influence of CECM on the rheological characteristics of GelMA hydrogel is shown in Figure 2A and B. Initially, the variation in hydrogels was caused by the sensitivity limit of the rheometer. With increasing oscillation frequency, the hydrogels sample reached a steady state. The G' of the CECM-GelMA gel was approximately 4979.64 Pa, and G" was approximately 132.66 Pa, which were determined by oscillation-time sweep measurements (Figure 2A). Compared with the G' and G" results of GelMA, two-way ANOVA showed that the G' and G" of CECM-GelMA hydrogels were significantly different. The dynamic strength of the composite hydrogel supplemented with CECM was significantly higher than that of the pure GelMA hydrogel. The G' value of the hydrogels increased (up to 1.9 times that of pure GelMA), while the G" value was lower than the G' value, indicating that the CECM-GelMA hydrogels showed a stronger elastic response at high shear rates. In addition, the ideal substitute material should have good thixotropy. The shear thinning behavior of hydrogels was confirmed by the dynamic viscosity curve in Figure 2B, where the connection between shear stress and shear rate was able to match the Herschel–Bulkley non-Newtonian fluid model[34]. It could be justified that the CECM-GelMA hydrogels display a higher total impedance as the dynamic shear angle frequency increases and have a stronger ability to maintain the shape in 3D printing. Therefore, bioinks that contain CECM are more biologically effective and have shown significant promise for use in 3D printing.

3.3.2. Mechanical test

Subsequently, the samples were tested by uniaxial compression experiments, and the effect of CECM content

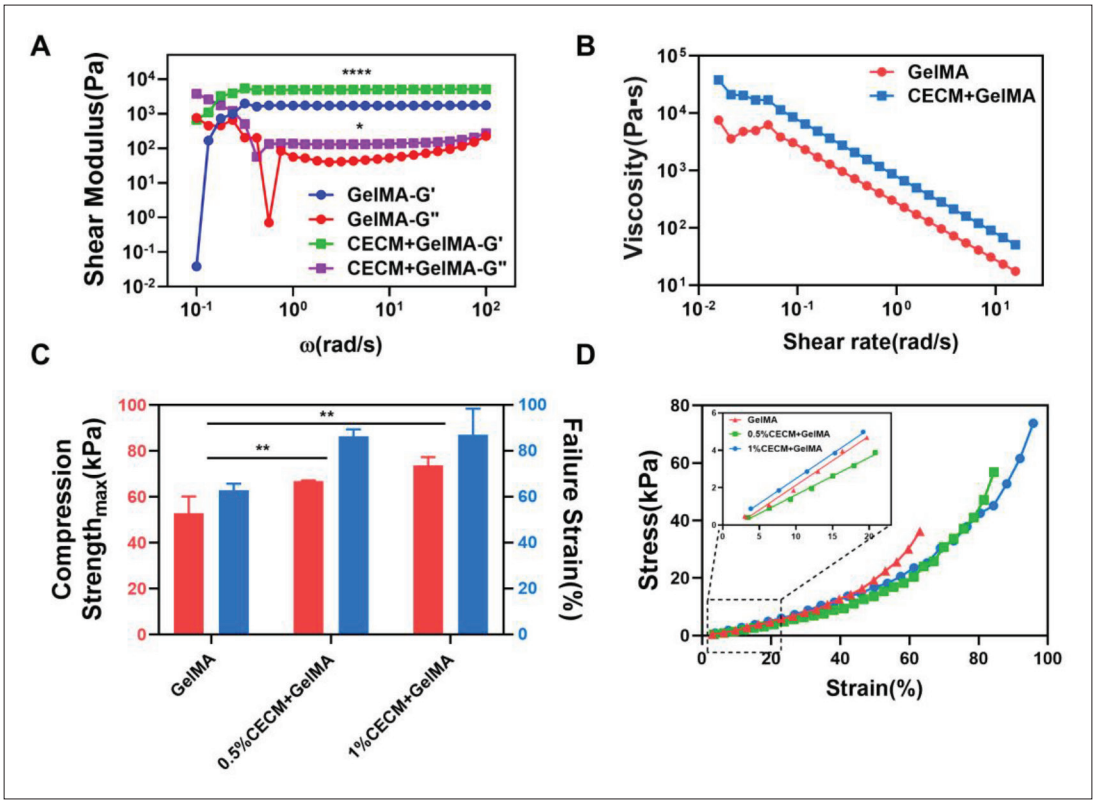

Figure 2. Mechanical properties of GelMA and CECM-GelMA hydrogels. (A) Storage modulus, loss modulus, and (B) complex viscosity of GelMA and 1%CECM-GelMA ($p < 0.01$). (C) Maximum compressive strength and failure strain. (D) Stress–strain curves of the compression test. The data (A–B) were subjected to two-way analysis of variance (ANOVA), and the data (C) were subjected to one-way ANOVA and are expressed as the mean ± standard deviation ($n = 3$; * $p < 0.05$, ** $p < 0.01$).

on the mechanical properties is shown in Figure 2C and D. Both the ductility and compressive strength of the samples were enhanced with increasing CECM concentration. The maximum compressive strength of hydrogels containing 1% (w/v) CECM reached 73.665 kPa, while the compressive strain at fracture increased from 62.84% to 87.02%. As shown in Figure 2D, the compression curve trends of the CECM-GelMA hydrogels and pure GelMA hydrogels were comparable. In the elastic deformation interval of 0%–20% strain, the material was within the elastic limit, and the modulus was characterized by the slope of the linear fit of this stage. It is calculated that the Young's modulus of the composite hydrogel reached 26.68 kPa, an increase of approximately 33.13%. In addition, uniaxial unmeasured compression tests were performed on the hCF-loaded CECM-GelMA samples cultured for 1 and 2 weeks. As shown in **Figure S3** (Supplementary File), after 2 weeks of culture, the hCF-loaded samples showed higher toughness and were able to withstand greater strain.

3.3.3. Degradation test

Then, the degradation result is shown in Figure 3A and B. The samples were soaked in PBS for *in situ* degradation. After being exposed to air for 4 h, the weight of the CECM-GelMA hydrogel was still maintained at ~83%, while that of pure GelMA dropped to 69%. The degradation rate of the hydrogels was evaluated by *in situ* degradation test, which showed that the composite hydrogels have good stability and durability.

However, under the action of collagenase (10 U/mL) solution, the collagenase degradation result is shown in Figure 3B. The degradation of the hydrogels in the *in vivo* environment was simulated by collagenase degradation test, which showed that both hydrogels could degrade rapidly under the action of type I collagenase, and the degradation rate of the composite hydrogels increased with time, indicating that the composite hydrogels could quickly give way to regenerated tissues during the tissue repair phase, with good biodegradability and biocompatibility.

3.3.4. Swelling test and water content

To evaluate the effect of CECM on water absorption, the kinetic curve of swelling was measured. As shown in Figure 3C, the lyophilized hydrogel swelled by water absorption in PBS buffer, and it swelled at a high speed

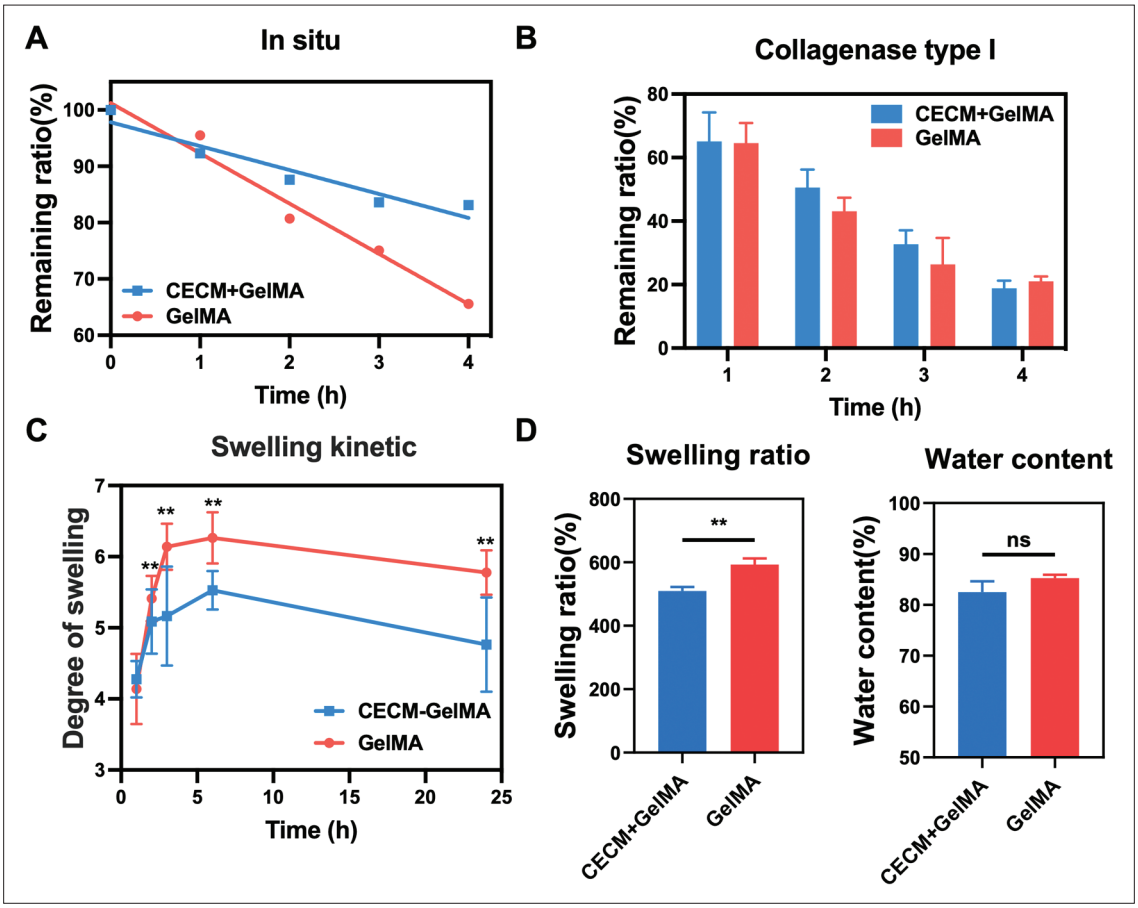

Figure 3. Physical properties of the GelMA and CECM-GelMA hydrogels. (A) *In situ* degradation in sample I (time: **, materials: ns); (B) degradation of collagenase type I (time: ****, materials: ns); (C) kinetic curve of swelling (time: **, materials: **); (D) the degree of swelling and water content (w/w) of the samples. The data (A–C) were subjected to two-way analysis of variance (ANOVA), and the data (D) were subjected to one-way ANOVA and are expressed as the mean ± standard deviation ($n = 3$; * $p < 0.05$, ** $p < 0.01$, **** $p < 0.0001$).

with increasing time. The growth rate was fast in the first 2 h, slowed down in 3–4 h, and then reached the swelling equilibrium state, and the swelling degree remained relatively stable. Therefore, the swelling rate of the composite hydrogel was 476% (Figure 3D). However, as shown in Figure 3D, the equilibrium water content of the two hydrogels was similar, and there was no significant difference. Compared with pure GelMA (~85%), the equilibrium water content of the CECM-GelMA group is 82%, which is closer to that of natural corneal (~78%) tissue. It can help to ensure the stability in the body fluid environment.

3.3.5. Transmittance

The transparency of the cornea is maintained by the regular arrangement of collagen fibers and stable corneal cells[35]. The cornea allows light with a wavelength of 365–2500 nm to pass through, and light with a wavelength below 365 nm has a weaker penetration and is mainly absorbed by the cornea to prevent UV damage to the eye. As shown in Figure 4, the spectral transmittance of the artificial cornea was measured. The transmittance of the prepared composite hydrogel in the visible light range of 400–700 nm showed an increasing trend (Figure 4A). In the blue-violet light waveband, the transmittance was low, which could reduce the damage of radiation to eyes. The transmittance of the sample gradually increased with increasing wavelength and remained stable, which was comparable to the human natural cornea in the relevant reference[36,37]. According to Figure 4B, after 2 weeks of culture on the hCF-loaded hydrogel, the spectral transmittance of the hydrogel was significantly improved in the range of 700–800 nm. By comparison, with the same sample thickness, the transparency of the CECM-GelMA hydrogel loaded with cells at 780 nm was 89.36%, while without cells, the transmittance was 75.26%. Then, one-way ANOVA of CECM/GelMA hydrogel samples with and without cells showed a significant difference in p value ($p = 0.0110$). Clearly, the light transmittance of the sample changed with the loaded cells.

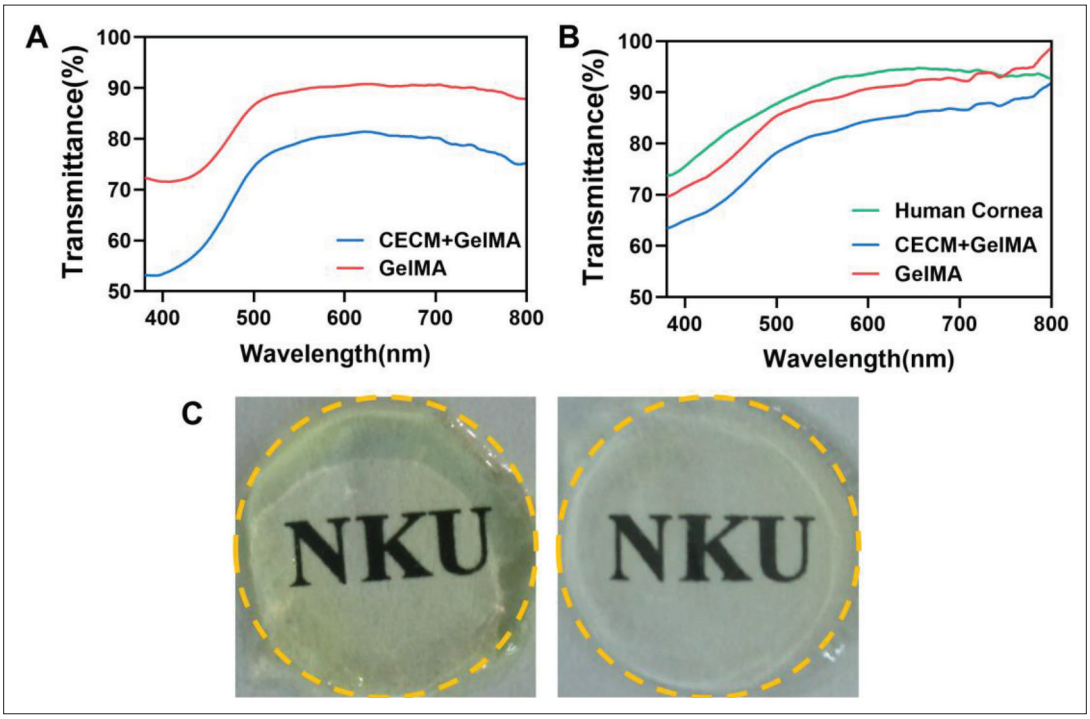

Figure 4. Transparency of the printed hydrogel. (A) Samples with no cells (materials: **, wavelength: ****); (B) cell-loaded samples cultured for 2 weeks (materials: **, wavelength: ****); (C) photographs showing the transparency of the printed GelMA hydrogel (left) and the printed CECM-GelMA hydrogel (right). The data (A–B) are expressed as the mean ± standard deviation and were analyzed using two-way ANOVA ($n = 5$, *$p < 0.05$, ** $p < 0.01$, **** $p < 0.0001$).

After that, the printed samples with printed curvature were placed on "NKU" text to see how visible it was. As shown in Figure 4C, the letters could be clearly seen through the printed corneas. At the same time, the smooth double-curvature shape allowed for the basic refraction of the cornea.

3.4. Biological characterization of the hydrogel

3.4.1. Live/dead analysis

The 3D image taken by confocal microscopy after the live/dead test is shown in Figure 5A. After 3D culture of hCFs, the results showed robust hCF survival in the composite hydrogel. Due to the role of CECM, the hCFs can survive and spread well in the interior as culture time increased Additionally, no sizable number of dead cells was found in the experimental samples after 14 days of growth. According to statistical calculations, the cell viability results are shown in Figure 5B ($n = 3$). In the 3D-printed hydrogel loaded with hCFs, CECM-GelMA (~75.29%) showed a higher viability than pure GelMA (~62.31%) on the first day after printing. After a longer culture, viability of hCFs in the CECM-GelMA group increased steadily (up to 94.84% after 2 weeks of culture), presumably due to the role of CECM. In contrast, the GelMA group showed a survival rate of 84.32% after 1 week of culture, with no significant changes thereafter. Meanwhile, cell migration toward the bottom of the dish was observed in the control group during the test, resulting in a lower number of cells in the hydrogel. These findings demonstrated that CECM provided a suitable microenvironment for the fabrication of functional artificial corneas, showing good cell viability of the composite hydrogels.

3.4.2. Immunofluorescence staining

In order to get closer to the complex 3D environment as cells reside *in vivo*, GelMA solution containing CECM and resuspended hCFs is printed. According to the immunofluorescence (IF) staining tests, corneal stromal functional protein (lumican) and corneal myofibroblast-specific marker (α-SMA) in the 3D-printed samples were detected. After 1, 7, and 14 days of culture, the results (Figure 6) showed that hCFs exhibited high expression of lumican (**Figure S8** in Supplementary File) and reduced expression of α-SMA in the composite hydrogels. Conversely, the IF results of GelMA samples showed that lumican was not detected and that α-SMA had low expression.

Furthermore, ALDH3A1, which is a protein mainly distributed in keratocytes and plays an important role in maintaining the normal structure and transparency of the cornea, was detected by immunofluorescence

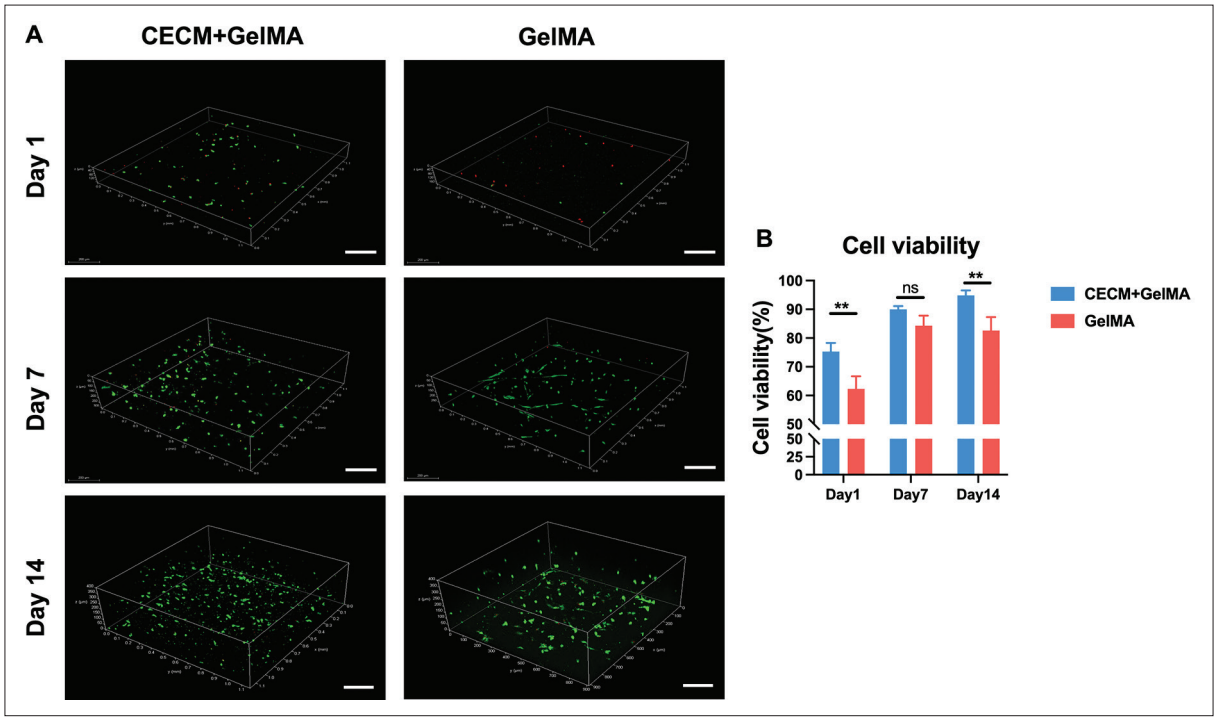

Figure 5. (A) Representative 3D live/dead stained confocal image of printed hCFs-loaded CECM-GelMA (CG) and GelMA hydrogels after 1, 7, and 14 days of incubation at 37°C. Live cells are stained with calcein-AM (green), and dead cells are stained with propidium iodide (red). The scale bar is 200 μm. (B) Statistics of cell viability of CECM-GelMA and GelMA hydrogels loaded with hCFs.

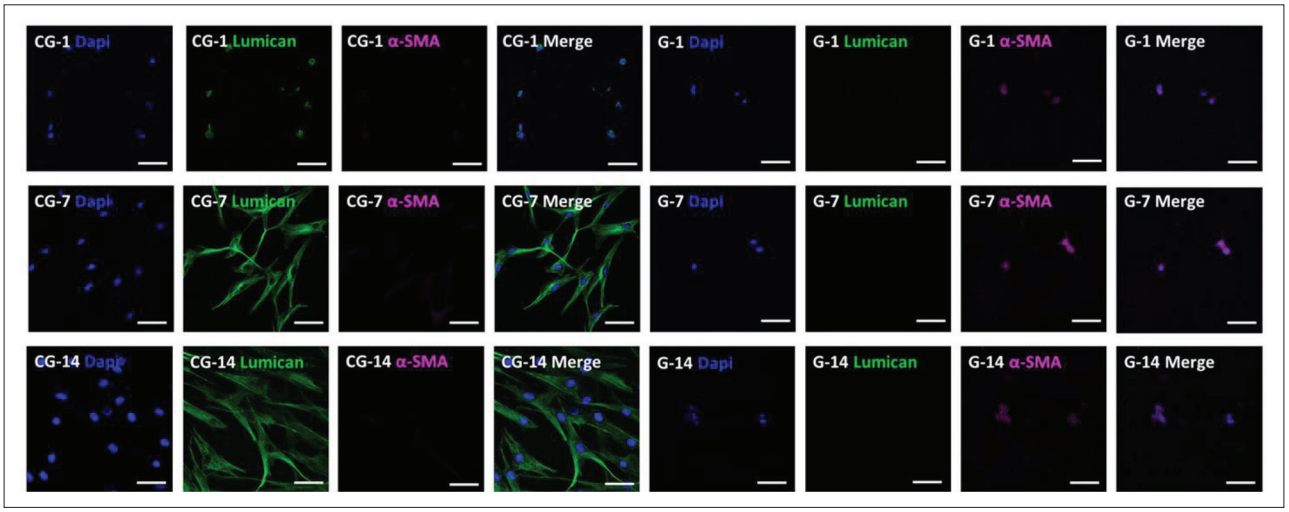

Figure 6. Confocal images of immunostained hCF-loaded bioprinted hydrogels on days 1, 7, and 14. Nucleus, myofibroblast-specific protein (α-SMA) and lumican are stained blue (by DAPI), magenta, and green, respectively. Contrast: pure GelMA hydrogel. The scale bar is 100 μm.

staining tests. According to Figure 7, ALDH3A1 was highly expressed in the CECM-GelMA hydrogels. In the control group, it was basically down-expressed (**Figure S8** in Supplementary File). In the following culture, the hCFs in the CECM-GelMA hydrogel showed more physiological morphology and formed cellular networks[38]. In addition, the 3D-bioprinted structure of CECM-GelMA also showed positive markers of collagen type I (Col-I) and vimentin (**Figure S5** in Supplementary File), indicating that the surrounding matrix of corneal fibroblasts contained important functional proteins such as Col-I and vimentin. The addition of CECM made the composite hydrogel closer to the composition of natural tissues and provided a suitable environment for cell growth.

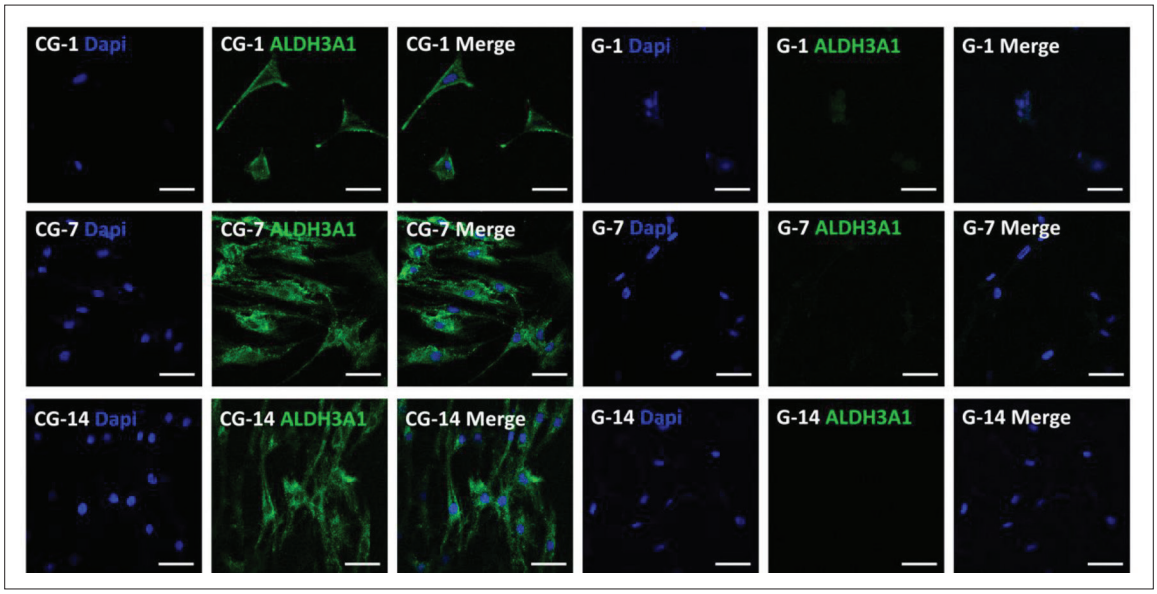

Figure 7. Confocal images of immunostained hCF-loaded bioprinted hydrogels on days 1, 7, and 14. Nucleus and keratocyte-specific protein (ALDH3A1) are stained blue and green, respectively. Contrast: pure GelMA hydrogel. The scale bar is 100 μm.

3.5. *In vivo* biocompatibility and therapeutic potential

3.5.1. Regeneration of corneal epithelium and corneal transparency

To evaluate the *in vivo* safety and outcome of CECM-GelMA hydrogel, the biocompatibility and therapeutic potential of the CECM-GelMA hydrogel were studied in a focal corneal defect model with the corneal defects of 5 mm diameter and 1/3 the depth of the cornea. Focal corneal defects without hydrogel transplant and normal groups were used as controls. Schematic and surgical procedures are shown in Figure 8A.

During the follow-up, all rabbits with CECM-GelMA hydrogel transplant showed no inflammation or graft dislocation. Fluorescein staining images revealed that the defect area of the corneal epithelium gradually decreased over time in the CECM-GelMA group and almost re-epithelialize in 2 weeks, while the cornea was not yet re-epithelialize completely in 4 weeks in the control group (Figure 9A and B).

As shown in Figure 9B, the healing rate was 93.5% in CECM-GelMA group at 28 days post-operation, while the healing rate was 84% in control group (Figure 9B). There was a slight haze in the cornea of the CECM-GelMA group from 2 weeks to 4 weeks, but all rabbits recovered with favorable corneal transparency at 2 months, equivalent to the outcome of normal cornea (Figure 9A). Comparatively, the corneal defect group showed apparent corneal scar formation during the 2 months follow-up periods (Figure 9A). The AS-OCT results showed higher reflected signal in corneal stromal layer in corneal defect group than in CECM-GelMA group (Figure 8B), which demonstrated that the levels of corneal stromal haze and scarring were obviously higher in the corneal defect group than those observed in the CECM-GelMA group. The corneas were almost completely transparent 2 months after transplant of the CECM-GelMA hydrogels (Figures 8B and 9A).

3.5.2. Histological observation

The HE staining (Figure 10A) results further showed that the regenerated epithelium in the CECM-GelMA hydrogel group possessed a more regular arrangement than that observed in the control group. In addition, the superficial corneal stroma in the CECM-GelMA hydrogel group (Figure 10A) displayed regular structures similar to those in normal corneas. However, both the cell layers of epithelium and the keratocytes in superficial stroma were significantly increased in the control group compared with the normal group (Figure 10A part). At the same time, disordered arrangement of superficial fibers in the corneal stroma was observed (Figure 10A part). Moreover, the thickness of the corneal epithelial, stromal, and total thickness in the CECM-GelMA hydrogel group, control group, and normal group was histologically assessed at 2 months after surgery (Figure 10B). The results indicated no significant differences in the total thickness of the corneal among the groups. However, compared with the normal tissue (24.87 ± 4.19 μm), the control group exhibited a larger increase in the thickness of the corneal epithelial layer (52.71 ± 9.47 μm), demonstrating the occurrence of heterogeneous re-epithelialization in the control group. Nevertheless, the thickness of the corneal epithelial layer of CECM-GelMA hydrogel group (30.40 ±

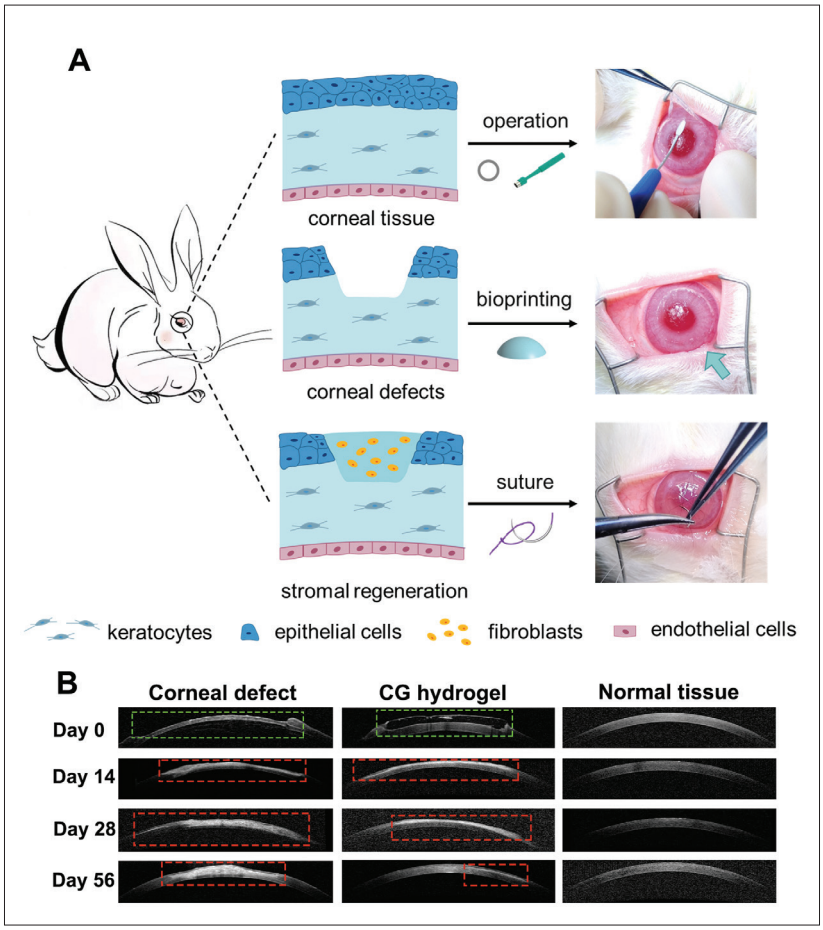

Figure 8. *In vivo* evaluation of the CECM-GelMA hydrogel scaffold in a rabbit model. (A) Schematic and surgical procedures for keratoplasty, including removal of specific parts of the corneal epithelium-stroma with a trephine, implantation of hydrogel, and covering with sutures. (B) Postoperative observation. AS-OCT images of corneal defect, CG hydrogel-treated, and normal tissue at 0, 2, 4, and 8 weeks after surgery. The defect area is marked with green frame, and scar area is mark with red frame.

5.63 μm) was slightly increased. The thickness of the stromal layers in the CECM-GelMA hydrogel group (316.09 ± 34.94 μm) was not significantly different from that of normal rabbit cornea (333.05 ± 28.38 μm), whereas the stromal layer in the control group could not regenerate properly and displayed a thinner thickness (304.17 ± 57.11 μm).

Furthermore, corneal haze and scarring were detected by analyzing the expression of the marker α-SMA in the IHC staining (Figure 10C). The IHC images showed positive expression of α-SMA in the control group but not in the CECM-GelMA hydrogel and normal group (Figure 10C and D). This indicated that the migration and residence of keratocytes were observed in the corneal stroma in control group.

4. Discussion

The ability to produce a tissue-specific artificial cornea has been made possible by the steady development of 3D bioprinting technology. Although the structures created in earlier studies had advantages and disadvantages of their own, creating smooth double-curvature shapes, intricate mechanical innovations, and microstructures remained difficult. In this work, we establish a hyperbolic biomimetic corneal structure using DLP-based 3D printing and propose a photocurable porcine CECM-GelMA bioink for the creation of artificial corneas.

It is generally known that the cornea of the human eye has the highest refractive power (approximately 43D) and that this ability is mostly influenced by the cornea's thickness and the optical interface's curvature. As a result, one of the keys is reconstructing the cornea's natural curvature. A customized artificial cornea model was created using computer-aided design modeling. After studying the printability of the bioink, the effects of the print layer thickness and exposure time on the structure of the bioink were explored for the same concentration and power density, as shown in **Figure S7** (Supplementary

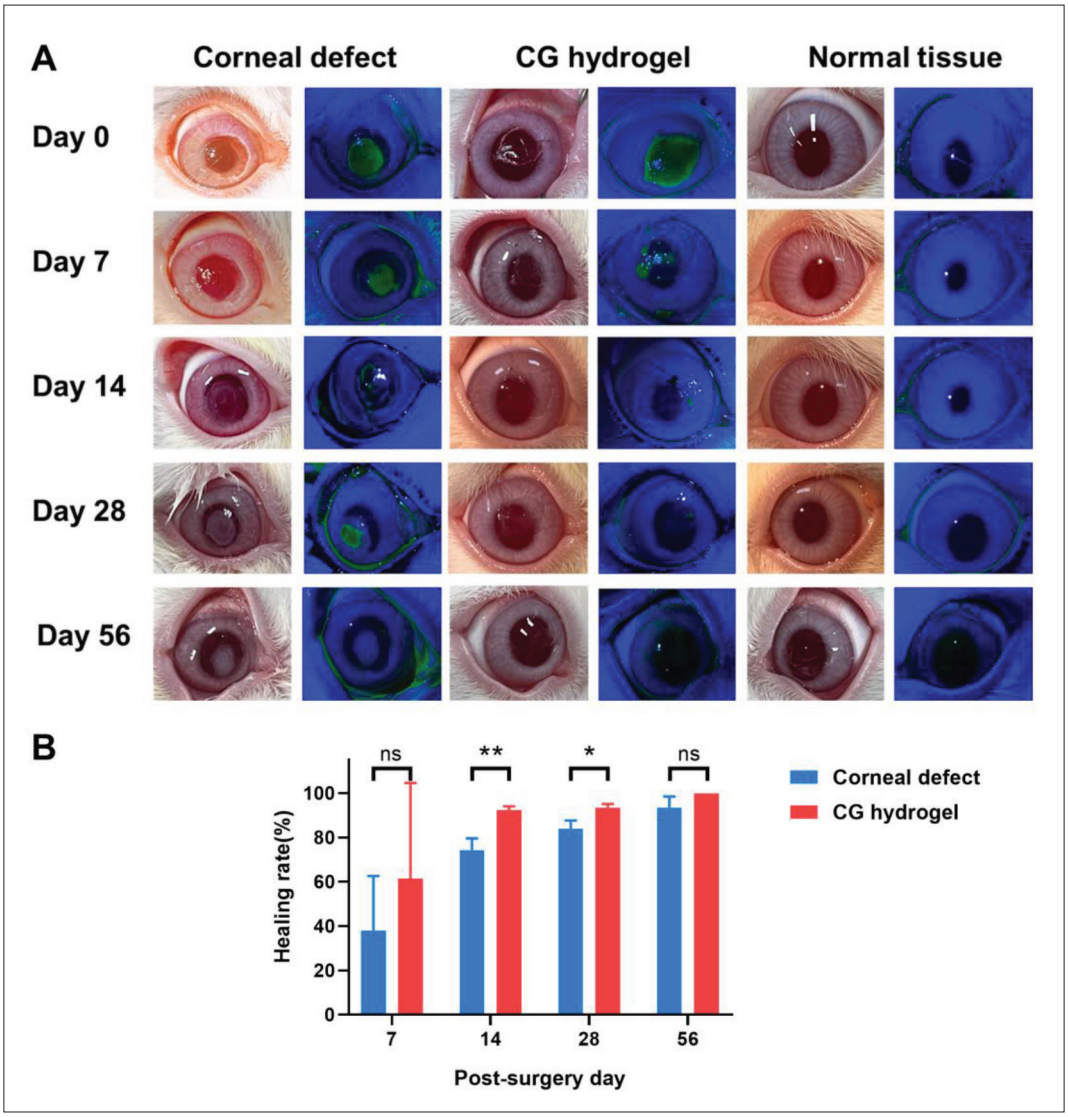

Figure 9. D-Luciferin experiment verifies epithelial regeneration after *in vivo* corneal defect. (A) Slit-lamp observations and fluoresce in staining images of corneal defect, CG hydrogel-treated, and normal tissue at 0, 2, 4, and 8 weeks after surgery. (B) Quantitative results of corneal epithelial repair area in *in vivo* model.

File). Following extensive testing, the ideal material composition and printing parameters were found, and the manufacturing of corneal alternatives continued, using a homemade DLP 3D bioprinting system to create the appropriate structure. Since most photoinitiators used in photopolymerization are cytotoxic, the CCK-8 kit was used to investigate the effect of 0.5% LAP on cell viability in the system (**Figure S4** in Supplementary File). GelMA samples cured with LAP have negligible effects on cell viability after crosslinking, and the overall cell viability is good within a short printing time (<60 min) and low photoinitiator concentration (<0.5% (w/v))[39]. Then, considering that GelMA is a relatively transparent solution, the vertical accuracy is determined by tartrazine, which is a biocompatible UV light absorber. The absorption spectrum of tartrazine was measured (**Figure S2** in Supplementary File), which indicated that tartrazine had obvious absorption in the UV band. The absorbance of the absorbent at different concentrations was measured by a microplate reader (800TS, Bio Tek Instruments Inc., USA) to obtain the molar absorption coefficient. Considering both the printing layer and cell viability, the UV absorbent concentration should be adjusted to achieve a proper crosslinking depth.

According to previous reports, the accuracy of hydrogel printing is difficult to determine. Unlike resins that can be inspected by contact inspection or scanning electron

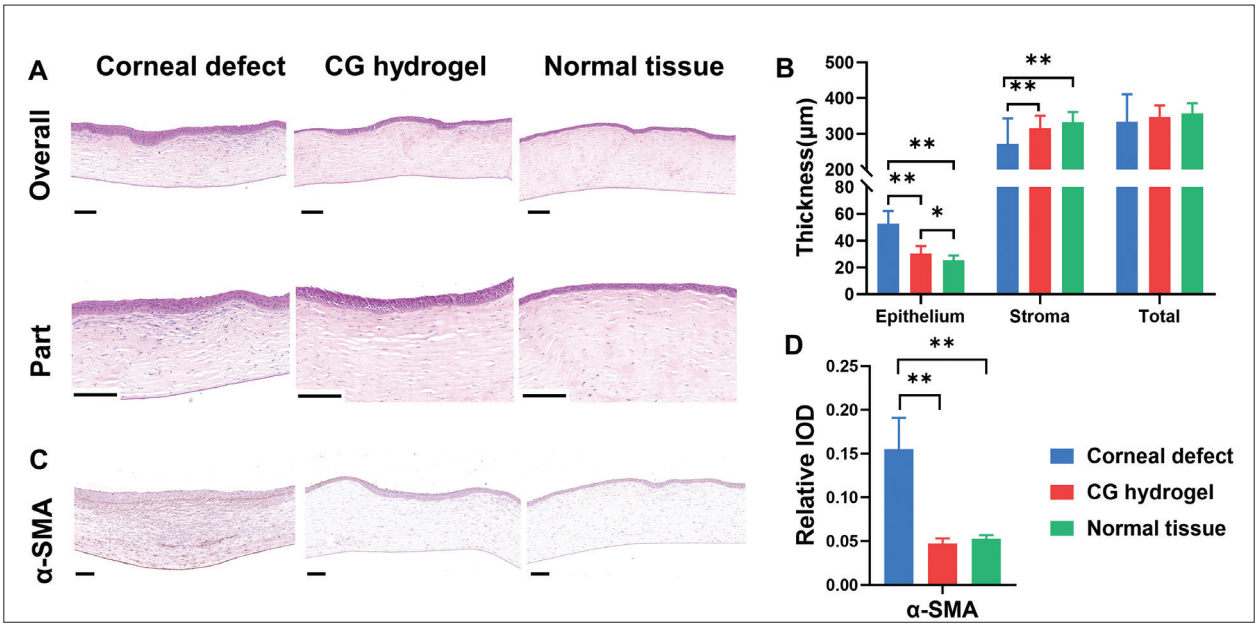

Figure 10. (A) HE staining images of corneal defect, CG hydrogel-treated, and normal tissue at 8 weeks after surgery. (B) Quantitative results(epithelial, stroma, and total thickness) of repaired cornea (* $p < 0.05$, ** $p < 0.01$; experiment: CG hydrogel; control: corneal defect and normal tissue). The scale bar of overall is 200 μm; and the scale bar of part is 100 μm.(C) IHC staining images of corneal defect, CG hydrogel-treated, and normal tissue at 8 weeks after surgery (* $p < 0.05$, ** $p < 0.01$). (D) Quantification of IHC staining results (experiment: CG hydrogel; control: corneal defect and normal tissue). Scale bars = 100 μm.

microscope (SEM), hydrogels have a soft surface and high-water content. Traditional measurement methods cannot be utilized[40]. As shown by the imaging findings of OCT scanning (Figure 1), the manufactured artificial cornea has a smooth hyperbolic structure, achieving a biomimetic shape. Although on-demand[41], extrusion-based printing, and mold construction[37] have shown better single-curvature results, this automated, free-form construction will be more attractive for customized manufacturing.

On the foundation of form bionics, the creation of a natural corneal microenvironment is also crucial. Based on the photocurable properties of GelMA, it is considered to be a popular hydrogel material in the field of tissue engineering. However, it has poor robustness and a narrow stiffness range and needs to be compounded with other materials to achieve corresponding performance. Moreover, dECM, which has excellent physical properties and a wide range of biochemical factors, has recently become widely accepted as the best material for simulating complex natural microenvironments and has considerable potential for tissue regeneration and biochemical environment reconstruction[42]. To impart high biocompatibility and photocurable ability, a functional bioink with a unique microenvironment, GelMA mixed with CECM, was created, which can build corneal tissue with highly adjustable mechanical properties. Although the covalent bonds formed during the photocurable process of GelMA hydrogels are strong, in hydrogels with a high degree of modification, the increase in the degree of crosslinking will lead to an increase in the brittleness of the material. Overall, in rheological experiments, CECM-GelMA hydrogels showed weak shear frequency dependency, higher gel strength, and shorter viscoelastic chain sizes (Figure 2A and B). The rheological behavior remains in a steady state[43]. Since parameters such as the size of the indentation tip, the depth of the indentation, the sample size, and the loading speed affect the results of the compression test[44], this leads to a huge difference in the compressive modulus of the cornea (the average compression modulus of the natural cornea is from 3.54 ± 0.30 MPa[45] to 3.06~26.38 kPa[46]).

The findings of the subsequent uniaxial compression test in our study served as additional confirmation of the excellent mechanical qualities of the composite hydrogels (Figure 2C and D). Afterward, the promotion in compression of CECM-GelMA is caused by a combination of many factors. Bioink based on CECM is rich in collagen, which is responsible for conferring strength and elasticity, so it is easy to form physical crosslinks through intermolecular interactions. CECM can provide proteoglycans and elastin that confer viscoelastic properties to the whole cornea[47]. Due to the extremely low number of polar residues in elastin and the resistance due to attachments between proteoglycans or other matrix

proteins and the microstructure, the chemical stability of hydrogels is increased[48-51]. These findings show that the composite hydrogel has enhanced deformation resistance and high resilience, making it a viable material for prosthetic corneas.

Then, additional crucial characteristics required for artificial corneas were examined. Initially, the *in vitro in situ* degradation and collagenase degradation experiments of GelMA and CECM-GelMA hydrogels followed similar rules. The higher degradation rate of the CECM-GelMA hydrogel indicates that it contains segments of collagen peptides that are vulnerable to proteases[52]. The incorporation of natural corneal extracellular matrix makes the hydrogels adjust biodegradability. This also indicates that CECM contains more protein molecules, such as collagen and proteoglycans, and has more cleavable sites. However, when PBS is used for *in situ* degradation, the presence of CECM reduces the degree of *in situ* degradation and enhances the stability of the hydrogel against environmental attacks (Figure 3A and B). Next, in the swelling experiment, the CECM-GelMA hydrogel had a lower swelling rate. This may be due to the fact that the CECM contains biologically active molecules, such as structural proteins and chitosan, which are cross-wound inside the hydrogel structure and make the composite hydrogel structure more compact. Therefore, the crosslinked network in the blended hydrogels makes it difficult for water to diffuse. It is revealed that for a lower swelling rate, the samples produce less deformation (Figure 3C and D).

Furthermore, one of the crucial factors is the transmittance of the artificial cornea. Upon testing, the transparency of the sample containing 1% (w/v) CECM was lower than that of pure GelMA (Figure 4). Due to the blending of CECM, the optical homogeneity decreased, and the light scattering increased. However, compared with the transmittance of traditionally prepared keratoprostheses containing CECM[53], which is approximately 50%, the transmittance of the CECM-GelMA hydrogel can be stabilized at ~86% in the wavelength range greater than 500 nm. Although the CECM-GelMA hydrogel did not achieve more than 90% light transmittance of the pure GelMA hydrogel, it still had better light transmittance than other artificial corneas[54]. Notably, the spectral transmittance of the hydrogel changed after 2 weeks of culture on the hCF-loaded hydrogel (Figure 4B). After analysis, the result may be due to the vigorous functional activity of hCFs, with obvious protein synthesis and secretion activities, which increases the colloidal osmotic pressure of the hCF-loaded samples and plays an important role in maintaining the water balance of the samples. With increasing colloid osmotic pressure, the light transmittance of the sample is improved to a certain extent.

Several studies have indicated that growth factors hold the key components that regulate cell fate in the process of tissue regeneration. The corneal decellularized extracellular matrix retains most of the ECM components of natural tissues[55], which can be used to 3D print and embed corneal cells. Counterintuitively, the addition of CECM allowed the population of cells retained in the hydrogels to better mimic the native tissue environment compared to pure GelMA. According to Figure 5A, hCFs loaded in the GelMA hydrogels were distributed in the bottom layer of the sample after 2 weeks of cultivation. Due to the durotaxis and mechanosensing of fibroblasts, the hCFs in the GelMA hydrogel crawled out, reducing the number of internal cells. However, due to the role of CECM, the internal environment of the CECM-GelMA hydrogel is more suitable, and the hCFs can survive and spread well in the interior, showing higher cell activity, as shown in Figure 5B. However, the hCFs in the CECM-GelMA hydrogel were cultured and distributed relatively uniformly. It was speculated that this may be because CECM exhibits its potential to survive cells from endogenous sources through a variety of mechanisms, including the release of matrix-bound growth factors. Subsequently, immunofluorescence staining analyses of essential proteins were carried out to determine the effects of scaled 3D architectures on cell function, motility, and differentiation. Lumican is a small leucine-rich proteoglycans (SLRPs) expressed in the corneal stroma that plays an important role in corneal transparency[56]. α-SMA is a specific protein of corneal myofibroblasts. Studies have shown that reversible transformation between keratocytes and corneal fibroblasts can occur, but if the stimulation is strong enough to transform into myofibroblasts, it is irreversible[57]. The hCFs in the composite hydrogel displayed upregulated expression of lumican and downregulated expression of α-SMA, while the control group showed the opposite (Figure 6). This shows that fibroblasts not only survive stably in CECM-GelMA hydrogels, but also do not undergo irreversible transformation to myofibroblasts and still maintain part of the function of keratocytes. Conversely, in response to such stimuli in GelMA hydrogels, hCFs were transformed into myofibroblasts expressing α-SMA[58].

Further research was performed on the impact of a 3D complex environment on hCFs. Among them, quiescent keratocytes express ALDH3A1 when they transform into corneal fibroblasts or myofibroblasts, which is accompanied by marked downregulation of ALDH3A1. Therefore, in the complex CECM-GelMA surroundings, hCFs secreted proteoglycans such as ALDH3A1 (Figure 7), which is similar to resting keratocytes. At the same time, a similar behavior was also revealed in the expression of

other important proteins (**Figure S5** in Supplementary File). After culturing for several days, hCFs were in a stable state and did not transform into myofibroblasts. However, compared with pure GelMA hydrogel, CECM has a positive effect on the expression of keratinocyte markers and inhibits the transformation of fibroblasts into myofibroblasts *in vitro*[57].

In *in vivo* animal study, suitable bioprinted hydrogel substitutes were transplanted in rabbits with corneal defect (Figure 8A). After nearly 2 months of follow-up, the AS-OCT results demonstrated that the hydrogel could suitably fill with the defect and maintain the smooth surface (Figure 8B). During the corneal defect repair process, the experimental group transplanted with CECM-GelMA hydrogel achieved the restoration of matrix thickness and transparency, which inhibited the formation of corneal scarring compared with the corneal defect group (Figure 9). Moreover, collagen fiber structure and protein expression are crucial for preserving the clarity and functionality of the cornea[59,60]. HE and immunohistochemical stainings revealed that CECM-GelMA hydrogel had almost acquired the natural corneal effect after healing. Expression of key proteins such as α-SMA was downregulated (Figure 10).

Essentially, the mechanism of change in fibroblasts is unclear. Based on our experimental results, it is speculated that CECM-based composite corneal structures provide hCFs with positive microscopic guidance that enables them to naturally sense, respond to, and provide critical functionalities to the surrounding biophysical environment. These findings set the foundation for further research into artificial corneas with functionalities.

5. Conclusion

In summary, an artificial cornea with double curvature was fabricated by a homemade DLP 3D printing system. From a practical point of view, the morphology and surface topography of the corneal substitutes presented a smoother curvature surface and enable controllable customization. Notably, CECM-GelMA hydrogel as cornea-specific alternative exhibits favorable properties including high dynamic strength and compression stress, biocompatibility, and *in vivo* recoverability. Collectively, the artificial cornea manufactured by the DLP 3D system provides an effective alternative to ocular tissue and has potential application in the development of *in vitro* equivalents.

Acknowledgments

The authors of this work are deeply appreciative of the assistance received from professionals and personnel.

Funding

This work was supported by the National Key R&D Program of China (2021YFC2401400).

Conflict of interest

The authors declare no conflict of interest.

Author contributions

Conceptualization: Mingshan Zhang, Fang Yang, Qing Ye, Yan Wang
Data curation: Mingshan Zhang, Fang Yang, Yipeng Dong
Formal analysis: Mingshan Zhang, Fang Yang
Funding acquisition: Qing Ye
Investigation: Mingshan Zhang, Fang Yang, Shi-yao Zhang,
Methodology: Mingshan Zhang, Fang Yang, Shi-yao Zhang, Daobo Han
Project administration: Mingshan Zhang
Resources: Mingshan Zhang, Fang Yang, Shi-yao Zhang, Xinyun Li, Liyun Ling
Software: Daobo Han, Zhichao Deng
Supervision: Qing Ye, Yan Wang, Jianguo Tian, Xuewei Cao
Visualization: Mingshan Zhang, Fang Yang
Writing – original draft: Mingshan Zhang, Fang Yang
Writing – review & editing: Qing Ye, Yan Wang, Mingshan Zhang

Ethics approval and consent to participate

All animal experiments were approved by the Ethical Review Committee on the Welfare of Laboratory Animals of Hubei University of Medicine, China (No. 2021-084). All cell lines from human patients were approved by The Ethics Committee of Tianjin Eye Hospital, China (No. 2021-024). Patients agreed to donate lenticules following the small incision lenticule extraction (SMILE) surgery after informed consent was obtained from the patients.

Consent for publication

Not applicable.

Availability of data

Data will be made available on request.

References

1. de By T, 2003, Shortage in the face of plenty: Improving the allocation of corneas for transplantation. *Dev Ophthalmol,* 36: 56–61.
2. Gain P, Jullienne R, He Z, *et al.*, 2016, Global survey of corneal transplantation and eye banking. *JAMA Ophthalmol,* 134(2): 167–173.

3. Ruiz-Alonso S, Villate-Beitia I, Gallego I, *et al.*, 2021, Current insights into 3D bioprinting: An advanced approach for eye tissue regeneration. *Pharmaceutics,* 13(3): 308.

4. Weng T, Zhang W, Xia Y, *et al.*, 2021, 3D bioprinting for skin tissue engineering: Current status and perspectives. *J Tissue Eng,* 12: 20417314211028574.

5. Zhang X, Liu Y, Luo C, *et al.*, 2021, Crosslinker-free silk/decellularized extracellular matrix porous bioink for 3D bioprinting-based cartilage tissue engineering. *Mater Sci Eng C,* 118: 111388.

6. Auger FA, Gibot L, Lacroix D, 2013, The pivotal role of vascularization in tissue engineering. *Annu Rev Biomed Eng,* 15(1): 177–200.

7. Mao Q, Wang Y, Li Y, *et al.*, 2020, Fabrication of liver microtissue with liver decellularized extracellular matrix (dECM) bioink by digital light processing (DLP) bioprinting. *Mater Sci Eng C,* 109: 110625.

8. Duarte Campos DF, Rohde M, Ross M, *et al.*, 2019, Corneal bioprinting utilizing collagen-based bioinks and primary human keratocytes. *J Biomed Mater Res A,* 107(9): 1945–1953.

   https://doi.org/10.1002/jbm.a.36702.

9. Zhang B, Xue Q, Hu HY, *et al.*, 2019, Integrated 3D bioprinting-based geometry-control strategy for fabricating corneal substitutes. *J Zhejiang Univ Sci B,* 20(12): 945–959.

   https://doi.org/10.1631/jzus.B1900190.

10. Li L, Lu C, Wang L, *et al.*, 2018, Gelatin-based photocurable hydrogels for corneal wound repair. *ACS Appl Mater Interfaces,* 10(16): 13283–13292.

11. Yu C, Ma X, Zhu W, *et al.*, 2019, Scanningless and continuous 3D bioprinting of human tissues with decellularized extracellular matrix. *Biomaterials,* 194: 1–13.

12. Zhang AP, Qu X, Soman P, *et al.*, 2012, Rapid fabrication of complex 3D extracellular microenvironments by dynamic optical projection stereolithography. *Adv Mater,* 24(31): 4266–4270.

13. Miotto M, Gouveia RM, Ionescu AM, *et al.*, 2019, 4D Corneal tissue engineering: achieving time-dependent tissue self-curvature through localized control of cell actuators. *Adv Funct Mater,* 29(8).10.1002/adfm.201807334.

    https://doi.org/10.1002/adfm.201807334.

14. Das S, Jang J, 2018, 3D bioprinting and decellularized ECM-based biomaterials for in vitro CV tissue engineering. *J 3D Print Med,* 2(2): 69–87.

15. Crapo PM, Gilbert TW, Badylak SF, 2011, An overview of tissue and whole organ decellularization processes. *Biomaterials,* 32(12): 3233–3243.

16. Nakayama KH, Batchelder CA, Lee CI, *et al.*, 2010, Decellularized rhesus monkey kidney as a three-dimensional scaffold for renal tissue engineering. *Tissue Eng Part A,* 16(7): 2207–2216.

17. Badylak SF, Freytes DO, Gilbert TW, 2009, Extracellular matrix as a biological scaffold material: Structure and function. *Acta Biomater,* 5(1): 1–13.

18. Lawrence BD, Marchant JK, Pindrus MA, *et al.*, 2009, Silk film biomaterials for cornea tissue engineering. *Biomaterials,* 30(7): 1299–1308.

19. Kilic Bektas C, Hasirci V, 2020, Cell loaded GelMA: HEMA IPN hydrogels for corneal stroma engineering. *J Mater Sc,* 31(1): 1–15.

20. He B, Wang J, Xie M, *et al.*, 2022, 3D printed biomimetic epithelium/stroma bilayer hydrogel implant for corneal regeneration. *Bioact Mater,* 17: 234–247.

21. Badylak SF, 2007, The extracellular matrix as a biologic scaffold material. *Biomaterials,* 28(25): 3587–3593.

22. Uyanıklar M, Gunal G, Tevlek A, *et al.*, 2019, Hybrid cornea: Cell laden hydrogel incorporated decellularized matrix. *ACS Biomater Sci Eng,* 6(1): 122–133.

23. Kim H, Park M-N, Kim J, *et al.*, 2019, Characterization of cornea-specific bioink: High transparency, improved in vivo safety. *J Tissue Eng,* 10: 2041731418823382.

24. Yazdanpanah G, Shen X, Nguyen T, *et al.*, 2022, A light-curable and tunable extracellular matrix hydrogel for in situ suture-free corneal repair. *Adv Funct Mater,* 32(24): 2113383.

25. Kim H, Jang J-H, Han W, *et al.*, 2023, Extracellular matrix-based sticky sealants for scar-free corneal tissue reconstruction. *Biomaterials,* 292: 121941.

26. Shen X, Li S, Zhao X, *et al.*, 2023, Dual-crosslinked regenerative hydrogel for sutureless long-term repair of corneal defect. *Bioact Mater*, 20(2023): 434–448.

27. Chen F, Le P, Lai K, *et al.*, 2020, Simultaneous interpenetrating polymer network of collagen and hyaluronic acid as an in situ-forming corneal defect filler. *Chem Mater,* 32(12): 5208–5216.

28. Rafat M, Jabbarvand M, Sharma N, *et al.*, 2023, Bioengineered corneal tissue for minimally invasive vision restoration in advanced keratoconus in two clinical cohorts. *Nat Biotechnol,* 41(1): 70–81.

29. Mao Q, Wang Y, Li Y, *et al.*, 2020, Fabrication of liver microtissue with liver decellularized extracellular matrix (dECM) bioink by digital light processing (DLP) bioprinting. *Mater Sci Eng C Mater Biol Appl,* 109: 110625.

    https://doi.org/10.1016/j.msec.2020.110625

30. Basara G, Ozcebe SG, Ellis BW, *et al.*, 2021, Tunable human myocardium derived decellularized extracellular matrix for 3D bioprinting and cardiac tissue engineering. *Gels,* 7(2): 70.

31. Petroll WM, Miron-Mendoza M, 2015, Mechanical interactions and crosstalk between corneal keratocytes and the extracellular matrix. *Exp Eye Res,* 133: 49–57.

32. Fernandez-Perez J, Ahearne M, 2019, Influence of biochemical cues in human corneal stromal cell phenotype. *Curr Eye Res,* 44(2): 135–146. 10.1080/02713683.2018.1536216

33. Harley BA, Leung JH, Silva EC, *et al.*, 2007, Mechanical characterization of collagen–glycosaminoglycan scaffolds. *Acta Biomater,* 3(4): 463–474.

34. Gan Y, 2012, Continuum mechanics: Progress in fundamentals and engineering applications, 10.5772/2103(Chapter 4).

35. Daxer A, Misof K, Grabner B, *et al.*, 1998, Collagen fibrils in the human corneal stroma: Structure and aging. *Investig Ophthalmol Vis Sci,* 39(3): 644–647.

36. Boettner EA, Wolter JR, 1962, Transmission of the ocular media. *Investig Ophthalmol Vis Sci*, 1: 776–783.

37. Peris-Martínez C, García-Domene MC, Penadés M, *et al.*, 2021, Spectral transmission of the human corneal layers. *J Clin Med,* 10(19): 4490.

38. Kong B, Chen Y, Liu R, *et al.*, 2020, Fiber reinforced GelMA hydrogel to induce the regeneration of corneal stroma. *Nat Commun,* 11(1): 1–12.

39. Nguyen AK, Goering PL, Reipa V, *et al.*, 2019, Toxicity and photosensitizing assessment of gelatin methacryloyl-based hydrogels photoinitiated with lithium phenyl-2, 4, 6-trimethylbenzoylphosphinate in human primary renal proximal tubule epithelial cells. *Biointerphases,* 14(2): 021007.

40. Sun Y, Yu K, Nie J, *et al.*, 2021, Modeling the printability of photocuring and strength adjustable hydrogel bioink during projection-based 3D bioprinting. *Biofabrication,* 13(3): 035032.

41. Duarte Campos DF, Rohde M, Ross M, *et al.*, 2019, Corneal bioprinting utilizing collagen-based bioinks and primary human keratocytes. *J Biomed Mater Res Part A,* 107(9): 1945–1953.

42. Kim BS, Das S, Jang J, *et al.*, 2020, Decellularized extracellular matrix-based bioinks for engineering tissue- and organ-specific microenvironments. *Chem Rev,* 120(19): 10608–10661.

43. Ranjan R, Rawat K, Bohidar H, 2016, Interface versus bulk gelation and UCST in hydrophobically assembled TX-100 molecular gels. *Colloids Surf,* 499: 113–122.

44. Hatami-Marbini H, Etebu E, 2013, Hydration dependent biomechanical properties of the corneal stroma. *Exp Eye Res,* 116: 47–54.

45. Sharifi S, Sharifi H, Guild C, *et al.*, 2021, Toward electron-beam sterilization of a pre-assembled Boston keratoprosthesis. *Ocul Surf,* 20: 176–184.

46. Petsche SJ, Chernyak D, Martiz J, *et al.*, 2012, Depth-dependent transverse shear properties of the human corneal stroma. *Investig Ophthalmol Vis Sci,* 53(2): 873–880.

47. Formisano N, van der Putten C, Grant R, *et al.*, 2021, Mechanical properties of bioengineered corneal stroma. *Adv Healthc Mater,* 10(20): 2100972.

48. Xu CC, Chan RW, Weinberger DG, *et al.*, 2010, A bovine acellular scaffold for vocal fold reconstruction in a rat model. *J Biomed Mater Res Part A,* 92(1): 18–32.

49. Parekh A, Mantle B, Banks J, *et al.*, 2009, Repair of the tympanic membrane with urinary bladder matrix. *Laryngoscope,* 119(6): 1206–1213.

50. Valentin JE, Turner NJ, Gilbert TW, *et al.*, 2010, Functional skeletal muscle formation with a biologic scaffold. *Biomaterials,* 31(29): 7475–7484.

51. Bron A, 2001, The architecture of the corneal stroma. BMJ Publishing Group Ltd, London, 379–381.

52. Harrington DJ, 1996, Bacterial collagenases and collagen-degrading enzymes and their potential role in human disease. *Infect Immun,* 64(6): 1885–1891.

53. Aldave AJ, Kamal KM, Vo RC, *et al.*, 2009, The Boston type I keratoprosthesis: Improving outcomes and expanding indications. *Ophthalmology,* 116(4): 640–651.

54. Ulag S, Uysal E, Bedir T, *et al.*, 2021, Recent developments and characterization techniques in 3D printing of corneal stroma tissue. *Polym Adv Technol,* 32(8): 3287–3296.

55. Ahearne M, Fernández-Pérez J, 2020, Fabrication of Corneal Extracellular Matrix-Derived Hydrogels. *Methods Mol Biol* 2145: 159-168.10.1007/978-1-0716-0599-8_11.

56. Chakravarti S, Petroll WM, Hassell JR, *et al.*, 2000, Corneal opacity in lumican-null mice: defects in collagen fibril structure and packing in the posterior stroma. *Invest Ophthalmol Vis Sci,* 41(11): 3365–3373.

57. Yamamoto M, Quantock AJ, Young RD, *et al.*, 2012, A selective inhibitor of the Rho kinase pathway, Y-27632, and its influence on wound healing in the corneal stroma. *Mol Vis,* 18: 1727–1739.

58. Jester JV, Barry-Lane PA, Cavanagh HD, *et al.*, 1996, Induction of α-smooth muscle actin expression and myofibroblast transformation in cultured corneal keratocytes. *Cornea,* 15(5): 505–516.

59. Wang F, Shi W, Li H, *et al.*, 2020, Decellularized porcine cornea-derived hydrogels for the regeneration of epithelium and stroma in focal corneal defects. *Ocul Surf,* 18(4): 748–760.

60. Scott S-G, Jun AS, Chakravarti S, 2011, Sphere formation from corneal keratocytes and phenotype specific markers. *Exp Eye Res,* 93(6): 898–905.